

Carboxymethyl cellulose: an efficient material in enhancing alternating current conductivity of HCl doped polyaniline

R. Megha · Y. T. Ravikiran · S. Kotresh · S. C. Vijaya Kumari ·
H. G. Raj Prakash · S. Thomas

Received: 28 August 2017 / Accepted: 11 December 2017 / Published online: 15 December 2017
© Springer Science+Business Media B.V., part of Springer Nature 2017

Abstract In the present research, to enhance the alternating current conductivity of polyaniline (PANI), carboxymethyl cellulose (CMC), a biopolymer, is used to prepare optimized polyaniline-carboxymethyl cellulose (PANI-CMC) composite. The composite was synthesized by in situ polymerization and then characterized by Fourier transform infrared spectroscopy (FTIR), X-ray diffraction (XRD) and scanning electron microscopy (SEM) techniques. Improvement in π -electron delocalization in the composite due to CMC was confirmed from FTIR studies. Decrease in d-spacing and inter-chain separation of PANI chains and increase in the degree of crystallinity of the composite, all determined from XRD studies suggested increase in conductivity of the

composite. SEM image of the composite has shown crumpled PANI on CMC forming a kind of network facilitating easier transport of charge carriers. Alternating current (AC) response characteristics of PANI-CMC composite were investigated in the frequency range 100 Hz–1 MHz and comparatively analyzed with those of pristine PANI. Increase in AC conductivity of PANI-CMC composite by one order magnitude as compared to that of PANI, mainly due to the presence of CMC in it, was confirmed experimentally. Decrease in density of states at Fermi level of PANI-CMC composite as compared to that of PANI calculated as per correlated barrier hopping model confirmed and supported experimentally observed increase in AC conductivity of the composite. So, CMC as a component of PANI based composites can effectively replace metals/metal oxides in increasing AC conductivity of such composites and has the potential for applications in electronic circuit elements and sensors.

R. Megha · Y. T. Ravikiran (✉) · S. Kotresh
Department of PG Studies and Research in Physics,
Government Science College, Chitradurga,
Karnataka 577 501, India
e-mail: ytrcta@gmail.com

S. C. Vijaya Kumari
Department of Physics, SJM College of Arts, Science and
Commerce, Chitradurga, Karnataka 577 501, India

H. G. Raj Prakash
Department of Physics, JNN College of Engineering,
Shivamogga, Karnataka 577 204, India

S. Thomas
International and Inter University Centre for Nanoscience
and Nanotechnology, Mahatma Gandhi University,
Kottayam, Kerala 686 560, India

Keywords Polyaniline · Carboxymethyl cellulose ·
AC conductivity · Correlated barrier hopping model

Introduction

Since the discovery of conducting polymers, their potential for technological applications is evolving mainly because of their ability to combine the

chemical properties of polymers with the electronic properties of metals/metal oxides and semiconductors (Kotresh et al. 2017; Basavaraja et al. 2008). The major advantage of these conducting polymers is the possibility of tuning their electrical properties by many routes such as doping, varying methods of preparation and their viability in preparing their blends and composites (Megha et al. 2017a). Such materials have found applications in super capacitors, electromagnetic shielding, catalysis and sensors etc. (Peng et al. 2016; Babayan et al. 2017; Mu et al. 2015; Kotresh et al. 2016a). Among the conducting polymers, polyaniline (PANI) has received considerable attention because of its unique characteristics like controllable chemical and electrical properties, simple preparation, low cost and excellent environmental stability. Because of all these properties, it has found wide variety of technological applications in many fields (Kotresh et al. 2015; Prasanna et al. 2016; Nagesh Sastry et al. 2013). In particular, researchers working on improving the conductivity of PANI make use of the unique feature of PANI chains—chemically flexible N–H group flanked on either side of phenylene ring (Fig. 1a) (Himanshu et al. 2011) and tune its electrical properties by different routes such as by synthesizing PANI using different methods or by ion beam irradiations or by incorporating PANI with suitable inorganic materials so as to enhance the scope of their applications. Some of the related works are reviewed here:

In a report by Hazarika et al. (2012) camphorsulfonic acid doped PANI has shown increase in conductivity when irradiated with increasing fluencies of radiations of Ni^{12+} ions of 160 MeV energy. According to a report by Megha et al. (2017a) AC

conductivity of PANI has increased, when n-type NiFeO_4 particles prepared by sol–gel auto combustion method were composited with it by insitu polymerization method to form optimized PANI- NiFeO_4 nanocomposite. AC conductivity of PANI has increased when gold nanoparticles prepared by colloidal dispersion method were composited with it by interfacial chemical polymerization method to form PANI-Au nanocomposite as reported by Bogdanovic et al. (2014). Nagaraju et al. (2015) have reported that AC conductivity of PANI has increased when it is composited with TiO_2 using camphorsulfonic acid as a dopant.

In all these works, though improvement in AC conductivity of PANI has been reportedly achieved, they suffer from some major disadvantages like use of chemicals which are expensive, less abundant and also not biocompatible and their methods of preparation are complex, in some cases requiring harmful radiations. So, in the present work, we aimed at overcoming these disadvantages simultaneously improving conductivity of PANI by incorporating it with a suitable biopolymer to form PANI-biopolymer hybrid system. Among such hybrids, cellulose as a biopolymer component is preferred because of its unique properties like renewability, biocompatibility, abundance, high specific strength and non-abrasiveness during processing (Ravikiran et al. 2014; Guo et al. 2013). Also, there are reports on the mechanical and electrical conductivity study of such cellulose based composites such as bacterial cellulose (BC) composited with conducting polymers like poly(3,4-ethylenedioxythiophene)-poly(styrenesulfonate)/polyaniline and also with metal oxides (Khan et al. 2015a; Feng et al. 2012; Jasim et al. 2017) and these composites have found applications in biomedical and optoelectronic fields (Khan et al. 2015b; Ul-Islam et al. 2014; Khan et al. 2015a). But in some cases, when BC is composited with conducting polymer by in situ polymerization method, BC matrix may get damaged and may limit their applications (Khan et al. 2015a). So, with all these perspectives, as a novel alternative, we considered carboxymethyl cellulose (CMC) to be composited with PANI. Moreover, CMC is water soluble polysaccharide cellulosic ether which can be extracted from the fibrous tissue of plants (Basavaraja et al. 2013). Also, CMC molecules can readily interact with host molecules to form a composite system due to the presence of carboxymethyl groups (Fig. 1b) with

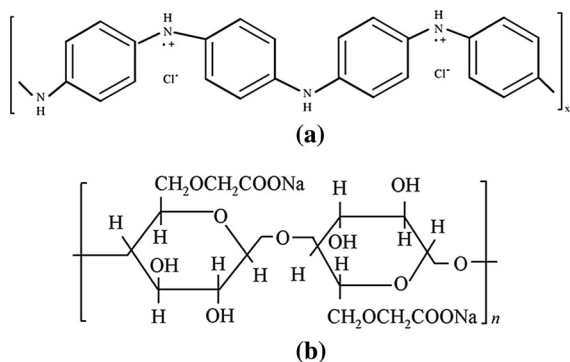


Fig. 1 Structure of *a* emeraldine salt form of PANI and *b* CMC

opposite electric charges in it and so would greatly contribute to synergistic effects in a composite system thus offering scope for tailoring their physical, and electrical properties (Guo et al. 2015; Abdel-Galil et al. 2014; El-Sayed and El-Gamal 2015).

So, as a first ever attempt, to exploit the advantageous properties of PANI and CMC to improve AC conductivity of PANI we have synthesized PANI-CMC composite by in situ polymerization method in which PANI acts as the host material and CMC as the supportive guest material. Then PANI, CMC and the composite were structurally characterized using FTIR, XRD and SEM techniques. Further to achieve best synergistic effects for maximizing conductivity, the concentration of CMC in the composite was optimized. Besides improving conductivity, the optimized composite is also expected to contribute towards improving efficiency and stability in multifunctional materials particularly in electronic circuit elements and sensors and thus would enhance the scope of its selection in such devices (Ravikiran et al. 2014; Megha et al. 2017a). To the best of our knowledge, this work is also the first ever attempt to study AC conductivity of PANI-CMC composite experimentally as well as theoretically through the parameters of correlated barrier hopping (CBH) model. Applications of this model throwing light on AC conductivity of such composites have been reported in recent literatures (Ghoswami et al. 2011; Mini et al. 2016). Such a study would provide an insight into the design of new materials and so would be beneficial in the selection of multifunctional materials in device technology (Megha et al. 2017b; Nandapure et al. 2013).

Materials and methods

Materials

Aniline [$C_6H_5NH_2$], ammonium persulfate [$(NH_4)_2S_2O_8$], hydrochloric acid [HCl] and carboxymethyl cellulose, all of analytical grade reagents, were purchased from S.D. Fine Chemicals, India. The aniline monomer was doubly distilled before use. De-ionized water was used throughout the synthesis work.

Preparation of PANI-CMC composite

The PANI-CMC composite was synthesized as follows: 0.6 g of CMC was dissolved in 180 ml de-ionized water at ambient temperature. 2.4 g aniline monomer and 60 ml of 1 M HCl solution were introduced into the above solution and the mixture was sonicated for 15 min to facilitate adsorption of aniline on CMC. With continuous stirring of the mixture, previously prepared 7.5 g ammonium persulfate in 60 ml de-ionized water was added drop wise into it and then was allowed to polymerize at room temperature for at least 8–10 h. The reaction product was collected by centrifugation and washed 5–6 times successively with 1 M HCl, de-ionized water and acetone until the filtrate became colorless. The filtrate is then dried in vacuum at 100 °C for 24 h when the required composite in the form of dark green powder was obtained. Pristine PANI was similarly synthesized under the same conditions but without CMC. The method of synthesis of PANI-CMC composite is illustrated in Fig. 2.

Characterization

The FTIR spectra of PANI, CMC and PANI-CMC composite were recorded in the range 400–4000 cm^{-1} using a Nicolet 750 FT-IR spectrometer (USA). For the purpose, each sample in powder form was dispersed in dry potassium bromide in the ratio 1:25 by weight and was ground to obtain uniform dispersion. Then the mixed powders of the samples were pressed separately in a cylindrical die to obtain transparent discs of approximately 1 mm thickness which were then exposed to IR radiations and the spectra recorded. The powder XRD patterns of PANI, CMC and PANI-CMC composite were recorded in the range $2\theta = 10^\circ$ – 80° using a Siemens D-5000 powder X-Ray diffractometer (Germany) with $CuK\alpha$ source radiation ($\lambda = 1.54 \times 10^{-10}$ m) at a scanning rate of 2° min^{-1} . The SEM images of the prepared PANI, CMC and PANI-CMC composite were recorded using an Hitachi S-520 scanning electron microscope (Japan). For recording the image, each powder sample was dispersed on the surface of carbon tape mounted on an aluminum tab and conducting gold was sputtered on the sample to avoid charging at the sample surfaces and hence selected areas were photographed.

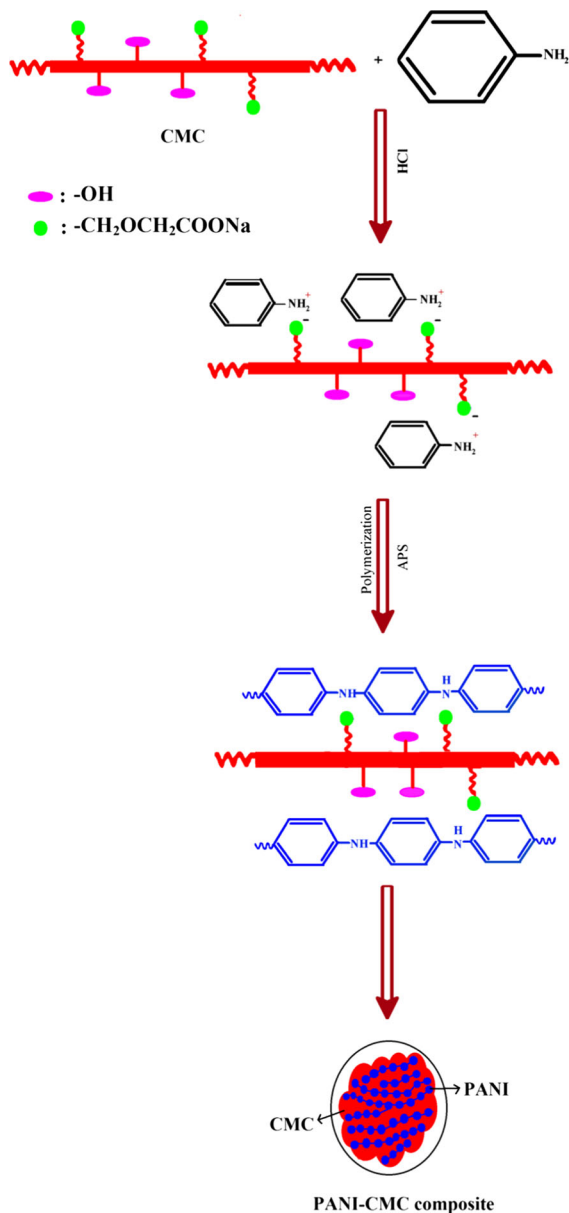


Fig. 2 The illustration of formation of PANI-CMC composite

The characteristic XRD parameters of CMC, PANI and PANI-CMC composite viz., d-space, inter-chain separation and degree of crystallinity were calculated using the formulae given below.

The d-spacing is estimated from the Bragg's relation (Bhadra et al. 2009)

$$n\lambda = 2d \sin \theta \quad (1)$$

The inter-chain separation length is estimated from the relation given by Klug and Alexander (Hazarika and Kumar 2016)

$$R = \frac{5}{8} \left[\frac{\lambda}{\sin \theta} \right] \quad (2)$$

The percentage of degree of crystallinity is calculated from the Eq. (3) (Hazarika and Kumar 2016)

$$K = \frac{A^I}{A^T} \times 100\% \quad (3)$$

where A^I is the area of broad diffraction peak and A^T is the total area under broad diffractogram.

AC response measurements

The AC response parameters of pristine PANI and PANI-CMC composite in the form of cylindrical pellets (0.8 cm dia × 1 mm thick, with silver paste electrodes) were studied using a Hioki Model 3532-50 programmable computer (Japan) interfaced with a digital LCR meter in the selected frequency range 100 Hz–1 MHz.

The real part of complex conductivity, complex permittivity, complex impedance and the imaginary part of complex impedance for pristine PANI and PANI-CMC composite were calculated using the formulae given below (Ravikiran et al. 2006).

$$\sigma'(\omega) = \omega \varepsilon_0 \varepsilon'' \quad (4)$$

$$\varepsilon' = C_p / C_0 \quad (5)$$

$$\varepsilon'' = \varepsilon' / \omega C_p R_p \text{ or } \varepsilon'' = \varepsilon' D \quad (6)$$

$$Z' = Z \cos \theta \quad (7)$$

$$Z'' = Z \sin \theta \quad (8)$$

where C_p is the equivalent parallel capacitance and $C_0 = (0.08854 \times A/t) \text{ pf}$, is the geometrical capacitance in vacuum with the same dimensions as that of the sample; A and t are the area and the thickness of the samples respectively; Z and θ are the impedance and the phase angle respectively.

Results and discussions

Fourier transform infrared spectroscopy

The FTIR spectra of PANI, CMC and PANI-CMC composite are shown in Fig. 3. In the FTIR spectrum of pristine PANI (Fig. 3a), the absorption bands at 3438, 1575, 1492, 1376, 1294, 1137 and 797 cm^{-1} are attributed to the PANI chain assigned respectively, to the N–H stretching of aromatic amine, C=C stretching deformation of quinoid rings, C=C stretching

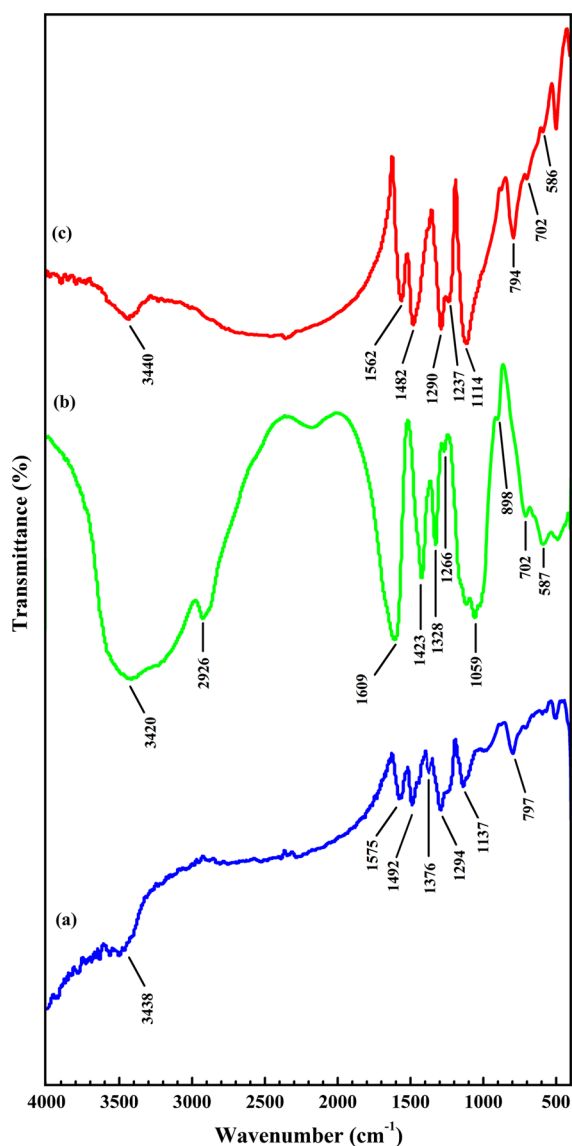
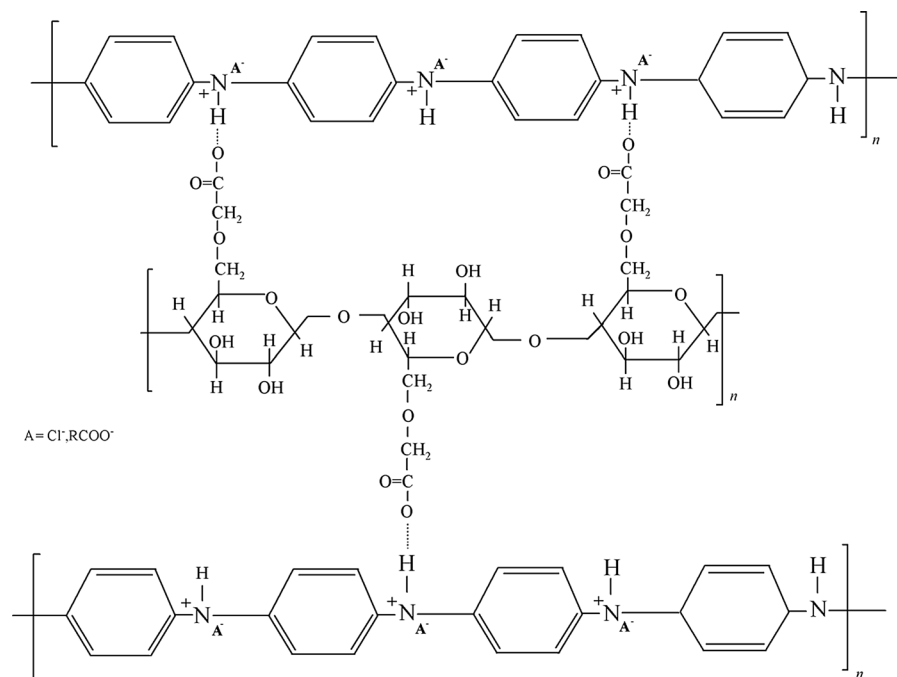


Fig. 3 Fourier transform infrared spectra of *a* pristine PANI, *b* CMC and *c* PANI-CMC composite

deformation of benzenoid rings, C–N stretching band of an aromatic amine, CCC ring in-plane deformation, in-plane bending vibration of C–H mode and out-of-plane deformation of C–H in the 1,4- disubstituted benzene ring of PANI respectively and all these band agree well with those published in literature (Gautam et al. 2016; Kotresh et al. 2016b). In particular, the appearance of band at 1492 cm^{-1} and relatively less absorption intensity band at 1575 cm^{-1} together with the appearance of band at 3438 cm^{-1} confirm emeraldine salt form of PANI (Ontolan et al. 2015; Khalid et al. 2014). The FTIR spectrum of CMC (Fig. 3b) shows strong absorption bands at 3420, 2926, 1609, 1423, 1328, 1266, 1059, 702 and 587 cm^{-1} which are the characteristic vibrations of CMC assigned respectively, to the O–H stretching vibration, the aliphatic C–H stretching vibration, the asymmetric stretching of carboxyl group ($-\text{COO}^-$), C–H stretching of $-\text{CH}_2$ group, OH bending vibration, alcohol C–OH stretching vibration, CHO– CH_2 stretching, ring stretching of α -D-(1-4) linkage and ring deformation of α -D-(1-6) linkage and all these have agreed well with those published in the literature (Hebeish et al. 2010; Gautam et al. 2016).

The FTIR spectrum of PANI-CMC composite (Fig. 3c) shows appearance of characteristic bands of both PANI and CMC with small shifts thus confirming the interaction of PANI with CMC during the formation of the composite (Gautam et al. 2016). The driving force for this interaction is the hydrogen bonding between the dopant ions of PANI and the polar molecules of CMC (Wheelwright et al. 2012). This interaction mechanism has been represented schematically in Fig. 4. Also, the variation in depth of characteristic bands of PANI in the composite—decrease in depth of 1290 cm^{-1} band and increase in depth of 1376 cm^{-1} —further confirm the formation of the integrated composite (Gautam et al. 2016). In addition, a greater depth in charge delocalization band of PANI in the composite at 1114 cm^{-1} indicating improved π -electron delocalization confirms increased conductivity of the composite. Similar observations for PANI in such composites have been reported in earlier literatures (Vijayakumar et al. 2012; Megha et al. 2017a). Further, the N–H band of PANI at 3438 cm^{-1} in the composite has not disappeared implying weak interaction between NH of PANI and carboxylic group of CMC in the composite. This suggests increase in electron density of PANI chains

Fig. 4 A schematic representation of mechanism of interaction between PANI and CMC



resulting in increase in conductivity of the composite (Ozkazanc et al. 2012; Sharma et al. 2009).

X-ray diffraction

The XRD patterns of PANI, CMC and PANI-CMC composite are shown in Fig. 5. The XRD pattern of pristine PANI (Fig. 5a) revealed some degree of crystallinity with the appearance of three broad peaks in the region of $2\theta = 15^\circ$ – 25° , similar to those observed in studies of PANI by others (Ravikiran et al. 2014). Among these peaks, the two minor peaks at $2\theta = 15^\circ$ and at $2\theta = 20^\circ$ assigned to (010) and (100) planes are attributed to periodicity parallel to the polymer chains and a major peak at $2\theta = 25^\circ$ assigned to (110) plane is attributed to periodicity perpendicular to the polymer chains. The CMC, a typically non-crystalline polymer (Fig. 5b) showed a broad peak at $2\theta = 20^\circ$, indicating its amorphous nature as is well established by the published literature (Upadhyaya et al. 2014; Basavaraja et al. 2012). The diffraction peaks of the PANI-CMC composite (Fig. 5c) were similar to those of pristine PANI and no obvious diffraction peak of CMC at about $2\theta = 20^\circ$ appeared which may be because the content of CMC in the composite was only about 20% and more likely because, the CMC might have dissolved uniformly in

PANI in the aqueous medium during the formation of the composite.

The respective numerical values of the XRD parameters of CMC, PANI and PANI-CMC composite calculated are given in Table 1. Significant revelations and hence inferences from the comparative analysis of the respective parameters of CMC, PANI and the composite are: As compared to those of PANI and CMC, the d-spacing and the inter-chain separation of PANI chains have decreased indicating improved π -electrons delocalisation, easier charge transport in it and hence increased conductivity of the composite (Vijayakumar et al. 2012). The calculated degree of crystallinity of pristine PANI and confirmed from reported literatures is 21% (Hazarika et al. 2012) while that of the composite is 25%. So it can be inferred that the relatively higher degree of crystallinity acquired by the composite has caused increase in its conductivity and is due mainly to the presence of CMC (Bhadra et al. 2009; Hazarika and Kumar 2016). This result also correlates very well with the result obtained from FTIR studies.

Scanning electron microscopy

The morphologies of CMC and the composite are shown in Fig. 6. The SEM image of CMC (Fig. 6a)

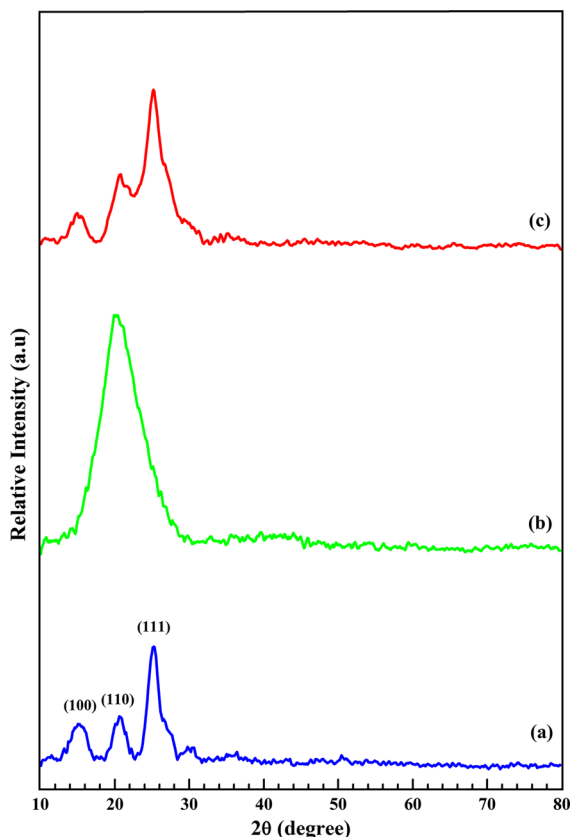


Fig. 5 X-ray diffraction patterns of *a* pristine PANI, *b* CMC and *c* PANI-CMC composite

Table 1 *d*-spacing (*d*), inter-chain separation (*R*) and degree of crystallinity (*K*) of CMC, pristine PANI and the composite

Samples	<i>d</i> (Å)	<i>R</i> (Å)	<i>K</i> (%)
CMC	4.36	5.45	—
PANI	4.28	5.35	21
PANI-CMC	4.27	5.33	25

reveals a uniform thick surface with various fractures (Kotresh et al. 2016a; Basavaraja et al. 2012).

The morphology of PANI-CMC composite (Fig. 6b) shows crumpled PANI on CMC thus forming a kind of network which might have facilitated easier transport of charge carriers causing increase in electrical conductivity of the composite. This composite showing such morphology has also been reported in literatures (Ravikiran et al. 2014; Basavaraja et al. 2013). As an extension of the morphological study, the

size of several grains of the composite were calculated using image J software and the average grain size was determined by the related number frequency histogram. The accuracy of average grain size was confirmed by applying log-normal distribution function (Fig. 6c). The average grain size so obtained was 120 nm.

AC response studies

The frequency dependence of AC conductivity of pristine PANI and the composite at 303 K are shown in Fig. 7. It is clear from the figure that the AC conductivity of the composite has increased as compared to that of PANI. This may be because, during the formation of the composite, HCl might have promoted the dissociation of neutral $-\text{COONa}$ of CMC into negatively charged $-\text{COO}^-$. The negatively charged CMC chains naturally get adsorbed to $-\text{NH}_2$ groups of the aniline monomer via electrostatic interaction. Thus the CMC might have served as a dopant for PANI during the polymerization of aniline, which might have promoted increase in conductivity of the composite (Peng et al. 2012).

This observed AC conductivity result can further be theoretically confirmed by fitting the experimentally measured AC conductivity data of pristine PANI and the PANI-CMC composite to CBH model and then studying the comparative variation in the parameters of CBH model as discussed below.

The plots of AC conductivity with frequency for PANI and the composite (Fig. 7) show two similar distinct trends in the measured frequency range 100 Hz–1 MHz: (1) the plot below the critical frequency showing conductivity independent of frequency-referred to as DC conductivity-due to long range motion of charge carriers and (2) the plot above the critical frequency indicating increase in conductivity with increase in frequency in accordance with the exponential power law-due to short range back and forth motion of charge carriers (Hazarika and Kumar 2014). These two trends appearing over the whole frequency range can be expressed by the general Eq. (9)

$$\sigma(\omega) = \sigma_{dc} + A\omega^s \quad (9)$$

where *A* is a temperature dependent pre-exponential factor and *s* is the frequency exponent lying between 0 and 1.

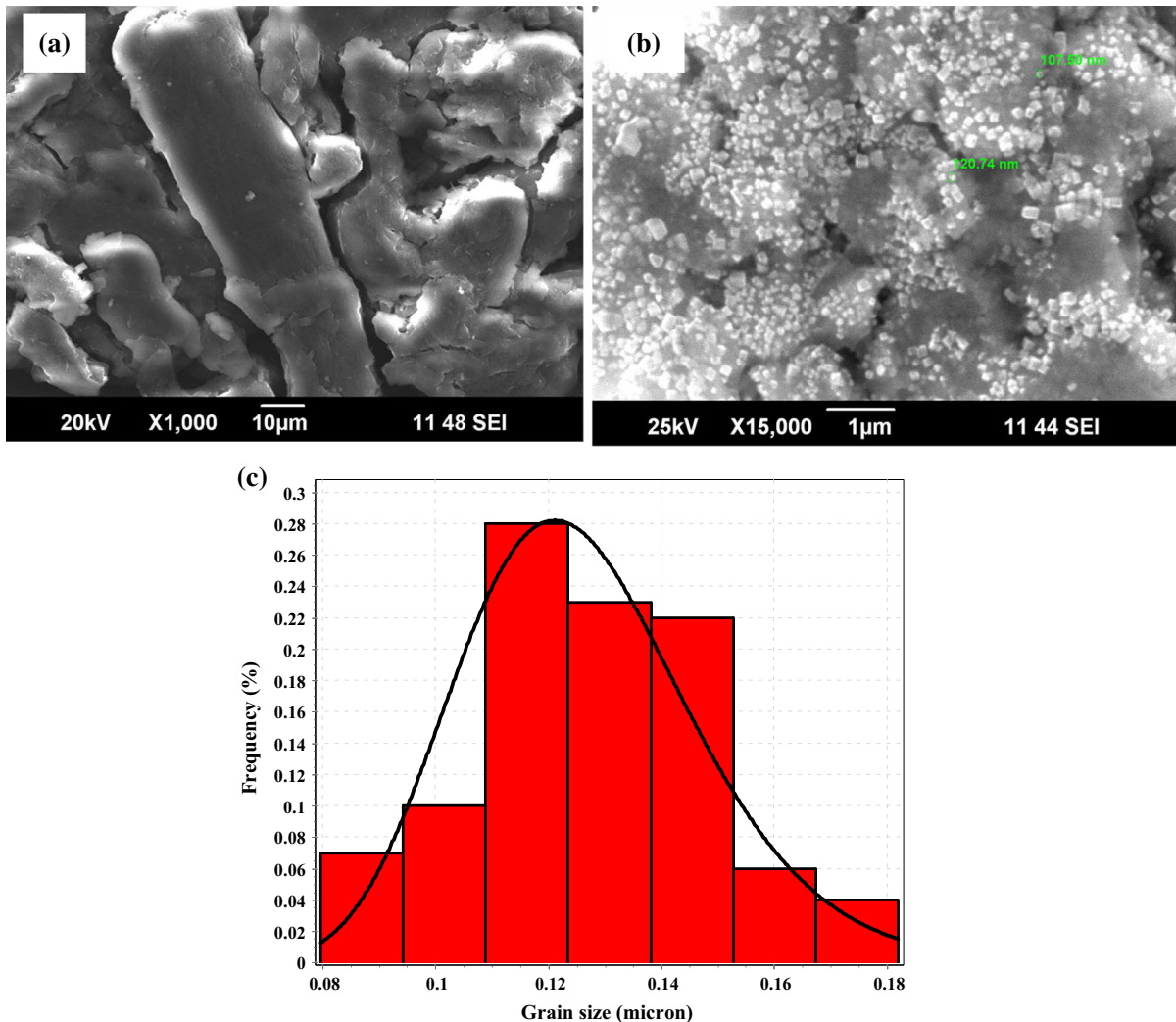


Fig. 6 Scanning electron micrographs of *a* CMC *b* PANI-CMC composite and *c* Number frequency (%) histograms showing grain size distribution of PANI-CMC composite, based on image analysis. Solid line is the best fit obtained using log-normal distribution

For applying a suitable theoretical model to understand the actual transport mechanism, the nature of variation of s with temperature is a determining factor. So the value of s for PANI and the composite was determined from the plot of experimentally obtained values of $\log \sigma(\omega)$ versus $\log \omega$. Then, the variation of s at different temperatures was studied and found that for both PANI and the composite, s decreased with increase in temperature (Fig. 8) decisively suggesting that AC conduction mechanism can be clearly understood through CBH model. The foundational aspect of this model is that charge transport is suggested to be due to thermal activation over the barrier between the

two sites, each having a coulombic potential well associated with it (Elliott 1987).

So as a first step in applying CBH model, binding energy as a function of temperature (for higher binding energies) for both PANI and the composite were obtained from the plot of $1-s$ versus T (Fig. 9) (Ozkazanc 2016) in accordance with the Eq. (10),

$$1 - s = \frac{6k_B T}{W_M} \quad (10)$$

Then, the hopping distance R_ω at a particular frequency ω and at a particular temperature T was calculated using the Eq. (11),

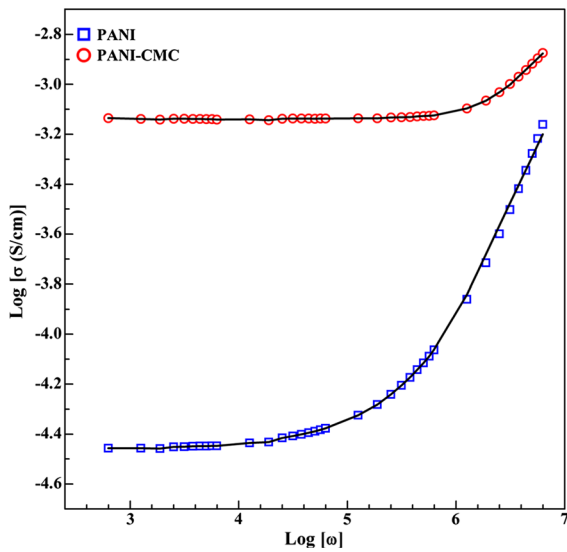


Fig. 7 Frequency dependence of AC conductivity of pristine PANI and the composite at 303 K. Solid lines are the best fits of Eq. (9)

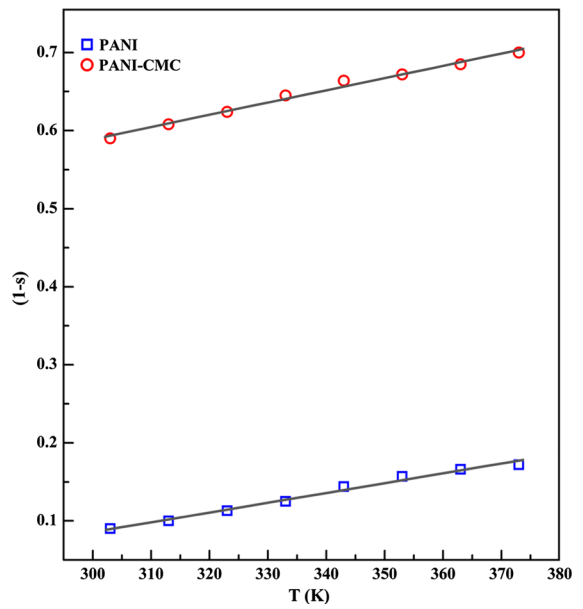


Fig. 9 Plots of 1-s versus T for pristine PANI and the composite

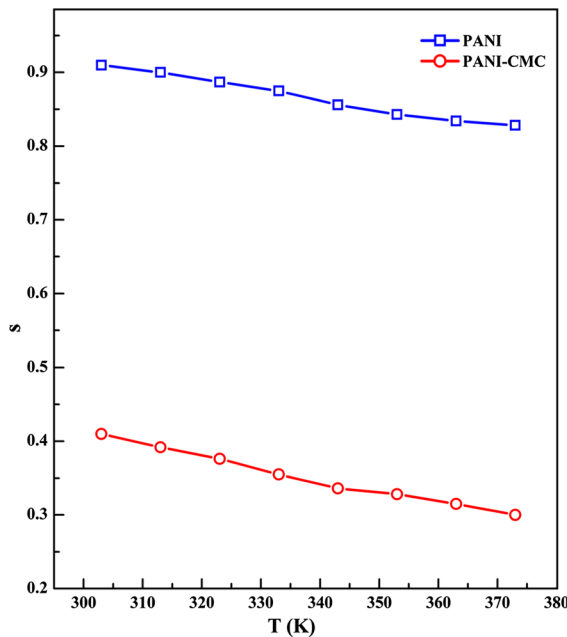


Fig. 8 Temperature dependence of frequency exponent s for pristine PANI and the composite

$$R_{\omega} = \frac{e^2}{\pi \epsilon \epsilon_0 [W_M - k_B T \ln(1/\omega \tau_0)]} \quad (11)$$

where e is the electron charge, ϵ_0 is the permittivity of free space and ϵ is the permittivity of the medium at a particular temperature and at a fixed frequency which

have been obtained experimentally from the plots shown in Fig. 10. A noteworthy inference from both the plots in Fig. 10 is that the permittivity has decreased with increase in frequency due to Maxwell–Wagner polarization which is also in conformity with the related earlier studies on such composites (Chitra et al. 2015).

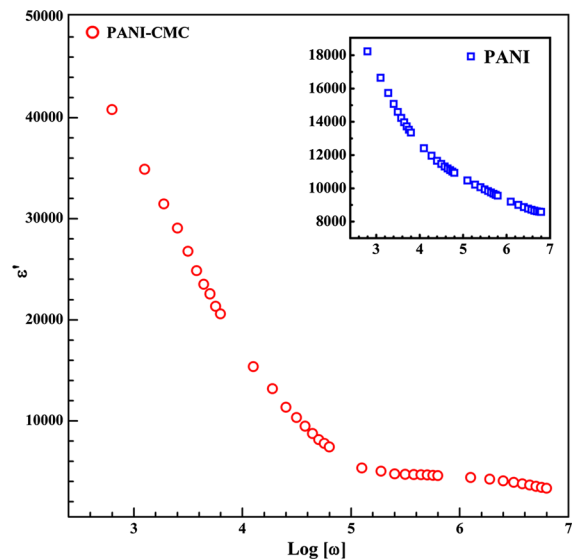


Fig. 10 Frequency dependence of real permittivity of PANI and the composite at 303 K

The characteristic relaxation time τ_0 at 303 K has been determined experimentally from the relaxation frequency peak ω_{\max} ($= 1/\tau_0$) (Ravikiran et al. 2006, Varade et al. 2013) of the complex plane impedance plot shown in Fig. 11. The value of τ_0 so obtained experimentally for PANI and the composite was used in Eq. (11) to calculate R_ω . It may be pointed out that the complex plane impedance plot for PANI and the composite is nearly a semicircle indicating absence of contact effects and is reminiscent of simple Debye model (Megha et al. 2017a). The semicircle plot also indicates that the contribution to conductivity from the grain boundaries is higher than that from its grains (Ravikiran et al. 2014).

Finally, the values of density of states $N(E_F)$ at Fermi level were calculated using the Eq. (12)

$$\sigma(\omega) = \frac{1}{24} \pi^3 N^2 \epsilon \epsilon_0 \omega R_\omega^6 \quad (12)$$

where $N = KTN(E_F)$, and values of $\sigma(\omega)$ for PANI and the composite have been obtained from the plot shown in Fig. 7.

The values of polaron binding energy W_M , hopping distance R_ω and the density of states $N(E_F)$ so calculated for PANI and the composite at 303 K and at 100 kHz are given in Table 2. From the analysis of this data, the following observations supporting the measured AC conductivity of PANI and the composite can be made: First, the calculated binding energy

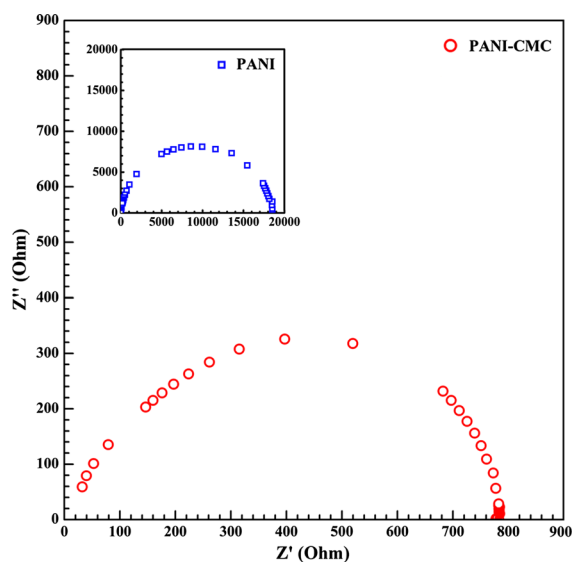


Fig. 11 Complex plane impedance plots of pristine PANI and the composite at 303 K

Table 2 Binding energy (W_M), hopping distance (R_ω) and density of states $N(E_F)$ of pristine PANI and the composite at 100 kHz and at 303 K

Samples	W_M (eV)	$R_\omega \times 10^{-2}$ (Å)	$N(E_F) \times 10^{27}$ (eV ⁻¹ cm ⁻³)
PANI	0.41	1.24	7.03
PANI-CMC	0.32	4.17	1.02

values of polarons of PANI and the composite are less than one, varying from 0.32 to 0.41 eV, confirming that the single polarons are the major charge carriers and not the bipolarons for which the binding energy would be four times higher (Banerjee and Kumar 2011; Chutia and Kumar 2014). Second, the binding energy of these single polarons of the composite is lesser than that of PANI implying lesser energy for hopping (Hazarika and Kumar 2016; Banerjee and Kumar 2010). Third, as compared to that of PANI, the hopping distance of polarons in the composite is longer which is attributed to the increased mobility of its charge carriers (Gmati et al. 2008). And fourth, the value of the density of states at Fermi level of the composite is lower as compared to that of PANI indicating increased delocalization of electronic states in its band gap (Banerjee and Kumar 2011; Banerjee and Kumar 2010). Thus, all the parameters of CBH model determined above summarily suggest increased conductivity of the composite as compared to that of PANI and so are in good agreement with the experimental result which also correlate very well with the structural characterizations studies.

Conclusions

The purpose of using a biopolymer CMC to make composite with PANI in order to improve AC conductivity of PANI has been achieved. The study establishes successful synergistic effects between the two components mainly because of the preparation of optimized PANI-CMC composite by simple in situ polymerization method. This work has also confirmed that CMC, apart from its role as a guest material in the composite also acts as a dopant which is advantageous as far as the processability of PANI is concerned as it avoids complex doping techniques thus saving cost and time. Another important feature of the work, a first

of its kind is the application of CBH model to understand charge transport mechanism in this composite in support of experimental AC conductivity measurements. Such an understanding through models would be helpful in selection of suitable materials for multifunctional devices.

Acknowledgments The authors are thankful to the University Grants Commission, New Delhi, for their financial support, provided under major research project (41-917/2012 (SR) dated: 23/07/2012) to carry out this work. This paper is a collaborative effort between Government Science College, Chitradurga and Mahatma Gandhi University, Kottayam-686 560, India. The authors also wish to acknowledge SAIF, Cochin, for providing facilities for structural characterization of the samples.

References

- Abdel-Galil A, Ali HE, Atta A, Balboul MR (2014) Influence of nanostructured TiO₂ additives on some physical characteristics of carboxymethyl cellulose (CMC). *J Radiat Res Appl Sci* 7:36–43
- Babayán V, Kazantseva NE, Moucka R, Stejskal J (2017) Electromagnetic shielding of polypyrrole-sawdust composites: polypyrrole globules and nanotubes. *Cellulose* 24:3445–3451
- Banerjee S, Kumar A (2010) Dielectric behavior and charge transport in polyaniline nanofiber reinforced PMMA composites. *J Phys Chem Solids* 71:381–388
- Banerjee S, Kumar A (2011) Dielectric spectroscopy for probing the relaxation and charge transport in polypyrrole nanofibers. *J Appl Phys* 109:1–9
- Basavaraja C, Veeranagouda Y, Lee K, Pierson R, Revanasiddappa HuhDS (2008) The study of DC conductivity for polyaniline-polymannuronate nano composites. *Bull Korean Chem Soc* 29:2423–2426
- Basavaraja C, Kim JK, Thinh PX, Huh DS (2012) Characterization and DC electrical conductivity of the composite films containing polyaniline-carboxymethyl cellulose. *J Polym Compos* 33:1541–1548
- Basavaraja C, Kim JK, Huh DS (2013) Characterization and temperature-dependent conductivity of polyaniline nanocomposites encapsulating gold nanoparticles on the surface of carboxymethyl cellulose. *Mater Sci Eng B* 178:167–173
- Bhadra S, Kim NH, Rhee KY, Lee J (2009) Preparation of nanosize polyaniline by solid-state polymerization and determination of crystal structure. *Polym Int* 58:1173–1180
- Bogdanovic U, Vodnik VV, Ahrenkiel SP, Stoilkovic M, Ciric-Marjanovic G, Nedeljkovic JM (2014) Interfacial synthesis and characterization of gold/polyaniline nanocomposites. *Synth Met* 195:122–131
- Chitra P, Muthusamy A, Dineshkumar S, Jayaprakash R, Chandrasekar J (2015) Temperature and frequency dependence on electrical properties of polyaniline/Ni_{(1-x)Co_xFe₂O₄} nanocomposites. *J Magn Magn Mater* 384:204–212
- Chutia P, Kumar A (2014) Electrical, optical and dielectric properties of HCl doped polyaniline nanorods. *Phys B* 436:200–207
- Elliott SR (1987) A.C. conduction in amorphous chalcogenide and pnictide semiconductors. *Adv Phys* 36:135–217
- El-Sayed AM, El-Gamal S (2015) Synthesis and investigation of the electrical and dielectric properties of CO₃O₄/(CMC + PVA) nanocomposite films. *J Polym Res* 22:1–12
- Feng Y, Zhang X, Shen Y, Yoshino K, Feng W (2012) A mechanically strong, flexible and conductive film based on bacterial cellulose/graphene nanocomposite. *Carbohydr Polym* 87:644–649
- Gautam V, Srivastava A, Pratap Singh K, Yadav VL (2016) Vibrational and gravimetric analysis of polyaniline/polysaccharide composite materials. *Polym sci ser A* 58:206–219
- Ghoswami M, Ghosh R, Chakraborty G, Gupta K, Meikap AK (2011) Optical and electrical properties of polyaniline-cadmium sulfide nanocomposite. *Polym Compos* 32:2017–2027
- Gmati F, Fattoum A, Bohli N, Mohamed AB (2008) Effects of the molar mass of the matrix on electrical properties, structure and morphology of plasticized PANI-PMMA blends. *J Phys Condens Matter* 20:125221–125229
- Guo B, Glavas L, Albertsson A (2013) Biodegradable and electrically conducting polymers for biomedical applications. *Prog Polym Sci* 38:1263–1286
- Guo X, Xue L, Lv W, Liu Q, Li R, Li Z, Wang J (2015) Facile synthesis of magnetic carboxymethylcellulose nanocarriers for Ph-responsive delivery of doxorubicin. *New J Chem* 39:7340–7347
- Hazarika J, Kumar A (2014) Enhanced AC conductivity and dielectric relaxation properties of polypyrrole nanoparticles irradiated with Ni¹²⁺ swift ions. *Nucl Instrum Methods Phys Res B* 333:73–79
- Hazarika J, Kumar A (2016) Studies of structural, optical, dielectric relaxation and ac conductivity of different alkybenzenesulfonic acids polypyrrole nanofibers. *Phys B* 481:268–279
- Hazarika J, Nath Chandrani, Kumar A (2012) 160 MeV Ni¹²⁺ ion irradiation effects on the dielectric properties of polyaniline nanotubes. *Nucl Instrum Methods Phys Res B* 288:74–80
- Hebeish A, Higazy A, El-Shafei A, Sharaf S (2010) Synthesis of carboxymethyl cellulose (CMC) and starch-based hybrids and their applications in flocculation and sizing. *Carbohydr Polym* 79:60–69
- Himanshu AK, Bandyopadhyay SK, Sen P, Mondal NN, Talpatra Taki GS, Sinha TP (2011) Electrical studies of low energy Ar⁹⁺ irradiated conducting polymer PANI-PVA. *Radia Phys Chem* 80:414–419
- Jaśim A, Ullah MW, Shi Z, Lin X, Yang G (2017) Fabrication of bacterial cellulose/polyaniline/single-walled carbon nanotubes membrane for potential application as biosensor. *Carbohydr Polym* 163:62–69
- Khalid M, Tumelero MA, Zoldan VC, Pla Cid CC, Franceschini DF, Timm RA, Kubota LT, Moshkalev SA, Pasa AA (2014) Polyaniline nanofibers-graphene oxide

- nanoplatelets composite thin film electrodes for electrochemical capacitors. *RSC Adv* 4:34168–34177
- Khan S, Ul-Islam M, Khattak WA, Ullah MW, Park JK (2015a) Bacterial cellulose-poly(3,4-ethylenedioxythiophene)-poly(styrenesulfonate) composites for optoelectronic applications. *Carbohydr Polym* 127:86–93
- Khan S, Ul-Islam M, Ullah MW, Kim Y, Park JK (2015b) Synthesis and characterization of a novel bacterial cellulose-poly(3,4-ethylenedioxythiophene)-poly(styrene sulfonate) composite for use in biomedical applications. *Cellulose* 22:2141–2148
- Kotresh S, Ravikiran YT, Raj Prakash HG, Ramana CHVV, Vijayakumari SC, Thomas S (2015) Polyaniline niobium pentoxide composite as humidity sensor at room temperature. *Adv Mater Lett* 6:641–645
- Kotresh S, Ravikiran YT, Raj Prakash HG, Ramana CHVV, Vijayakumari SC, Thomas S (2016a) Humidity sensing performance of spin coated polyaniline-carboxymethyl cellulose composite at room temperature. *Cellulose* 23:3177–3186
- Kotresh S, Ravikiran YT, Raj Prakash HG, Vijaya Kumari SC (2016b) Polyaniline-titanium dioxide composite as humidity sensor at room temperature. *Nanosystems: Physics, Chemistry, Mathematics* 7:732–739
- Kotresh S, Ravikiran YT, Tiwari SK, Vijaya Kumari SC (2017) Polyaniline-cadmium ferrite nanostructured composite for room-temperature liquefied petroleum gas sensing. *J Electron Mater* 46:5420–5447
- Megha R, Ravikiran YT, Vijaya Kumari SC, Thomas S (2017a) Influence of n-type nickel ferrite in enhancing the AC conductivity of optimized polyaniline-nickel ferrite nanocomposite. *Appl Phys A* 123:1–10
- Megha R, Kotresh S, Ravikiran YT, Ramana CHVV, Vijaya Kumari SC, Thomas S (2017b) Study of alternating current conduction mechanism in polypyrrole-magnesium ferrite hybrid nanocomposite through correlated barrier hopping model. *Compos Interfaces* 24:55–68
- Mini V, Archana K, Raghu S, Sharanappa C, Devendrappa H (2016) Nanostructured multifunctional core/shell ternary composite of polyaniline-chitosan-cobalt oxide: preparation, electrical and optical properties. *Mater Chem Phys* 170:90–98
- Mu B, Zheng Y, Wang A (2015) Facile fabrication of polyaniline/kapok fiber composites via a semidry method and application in adsorption and catalyst support. *Cellulose* 22:615–624
- Nagaraju SC, Aashis SR, Ramgopal G (2015) Conductivity of surface modified TiO₂ dope nanocomposites. *Measurements* 60:214–221
- Nagesh Sastry D, Revanasiddappa M, Basavaraja C, Suresh T, Raghavendra SC (2013) DC conductivity studies of doped polyaniline tungsten oxide nanocomposites. *Indian J Eng Mater Sci* 20:435–442
- Nandapure BI, Kondawar SB, Salunkhe MY, Nandapure AI (2013) Magnetic and transport properties of conducting polyaniline/nickel oxide nanocomposites. *Adv Mat Lett* 4:134–140
- Ontolan JPB, Alcantara PAM, Vequizo RM, Odarve MK, Sambo BRB (2015) Properties of in situ HCL-doped emeraldine polyaniline on n-Si (100) substrates for diode application. *Phys Status Solidi C* 12:580–583
- Ozkazanc H (2016) Characterization and charge transfer mechanism of PIN-CdSe nanocomposites. *Polym Compos* 37:3057–3065
- Ozkazanc E, Zor S, Ozkazanc H (2012) Synthesis, characterization, and AC conductivity of polyaniline/selenium composites. *J Macromol Sci B* 51:2122–2132
- Peng H, Ma G, Ying W, Wang A, Huang H, Lei Z (2012) In situ synthesis of polyaniline/sodium carboxymethyl cellulose nanorods for high-performance redox supercapacitors. *J Power Sour* 211:40–45
- Peng S, Fan L, Bao H, Zhang H, Xu W, Xu J (2016) Polypyrrole/nickel sulfide/bacterial cellulose nanofibrous composite membranes for flexible supercapacitor electrodes. *Cellulose* 23:2639–2651
- Prasanna BP, Avadhani DN, Muralidhara HB, Chaitra K, Thomas VR, Revanasiddappa Kathyayini N (2016) Synthesis of polyaniline/ZrO₂ nanocomposites and their performance in AC conductivity and electrochemical supercapacitance. *Bull Mater Sci* 39:667–675
- Ravikiran YT, Lagare MT, Sairam Mallikarjuna NN, Sreedhar B, Manohar S, MacDiarmid AG, Aminabhavi TM (2006) Synthesis, characterization and low frequency AC conduction of polyaniline/niobium pentoxide composites. *Synth Met* 156:1139–1147
- Ravikiran YT, Kotresh S, Vijayakumari SC, Thomas S (2014) Liquid petroleum gas sensing performance of polyaniline-carboxymethyl cellulose composite at room temperature. *Curr Appl Phys* 14:960–964
- Sharma BK, Khare N, Dhawan SK, Gupta HC (2009) Dielectric properties of nano ZnO-polyaniline composite in the microwave frequency range. *J Alloys Compd* 477:370–373
- Ul-Islam M, Khattak WA, Ullah MW, Khan S, Park JK (2014) Synthesis of regenerated bacterial cellulose-zinc oxide nanocomposite films for biomedical applications. *Cellulose* 21:433–447
- Upadhyaya L, Singh J, Agarwal V, Pandey AC, Verma SP, Das P, Tewari RP (2014) In situ grafted nanostructured ZnO/carboxymethyl cellulose nanocomposites for efficient delivery of curcumin to cancer. *J Polym Res* 21:1–9
- Varade V, Honnavar GV, Anjaneyulu P, Ramesh KP, Menon R (2013) Probing disorder and transport properties in polypyrrole thin-film devices by impedance and Raman spectroscopy. *J Phys D Appl Phys* 46:1–8
- Vijayakumar N, Subramanian E, Padiyan DP (2012) Change in AC conduction mechanism together with conversion of submicron to nanoparticles in polyaniline and its poly(vinyl pyrrolidone) blends on heating-induced water elimination. *Synth Met* 162:126–135
- Wheelwright VVK, Ray S, Easteal AJ (2012) Zein-polyaniline blends-a route to electrically conductive biopolymer. *Mol Cryst Liq Cryst* 554:252–263